DOI: 10.1002/chem.200700723

Homoleptic Copper(I) Arylthiolates as a New Class of p-Type Charge Carriers: Structures and Charge Mobility Studies

Chi-Ming Che,*[a, b] Cheng-Hui Li,[a, b] Stephen Sin-Yin Chui,[b] V. A. L. Roy,[b] and Kam-Hung Low[b]

Abstract: Polymeric homoleptic copper(I) arylthiolates $[Cu(p\text{-}SC_6H_4\text{-}X)]_\infty$ (X = CH_3 (**1**), H (**2**), CH_3O (**3**), *t*Bu (**4**), CF_3 (**5**), NO_2 (**6**), and COOH (**7**)) have been prepared as insoluble crystalline solids in good yields (75–95%). Structure determinations by powder X-ray diffraction analysis have revealed that **1**–**3** and **6** form polymers of infinite chain length, with the copper atoms bridged by arylthiolate ligands. Weak intra-chain π···π stacking interactions are present in **1**–**3**, as evidenced by the distances (3.210 Å in **1**, 3.016 Å in **2**, 3.401 Å in **3**) between the mean planes of neighboring phenyl rings. In the structure of **6**, the intra-chain π···π interactions (d = 3.711 Å) are insignificant and the chain polymers are associated through weak, non-covalent C–H···O hydrogen-bonding interactions (d = 2.586 Å). Samples of **1**–**7** in their polycrystalline forms proved to be thermally stable at 200–300 °C; their respective decomposition temperatures are around 100 °C higher than that of the aliphatic analogue $[Cu(SCH_3)]_\infty$. Data from in situ variable-temperature X-ray diffractometry measurements indicated that the structures of both **1** and **7** are thermally more robust than that of $[Cu(SCH_3)]_\infty$. TEM analysis revealed that the solid samples of **1**–**5** and $[Cu(SCH_3)]_\infty$ contained homogeneously dispersed crystalline nanorods with widths of 20–250 nm, whereas smaller plate-like nanocrystals were found for **6** and **7**. SAED data showed that the chain polymers of **1**–**3** and $[Cu(SCH_3)]_\infty$ similarly extend along the long axes of their nanorods. The nanorods of **1**–**5** and $[Cu(SCH_3)]_\infty$ have been found to exhibit p-type field-effect transistor behavior, with charge mobility (μ) values of 10^{-2}–10^{-5} $cm^2V^{-1}s^{-1}$. Polycrystalline solid samples of **6** and **7** each showed a low charge mobility ($< 10^{-6}$ $cm^2V^{-1}s^{-1}$). The charge mobility values of field-effect transistors made from crystalline nanorods of **1**–**3** and $[Cu(SCH_3)]_\infty$ could be correlated with their unique chain-like copper–sulfur networks, with the *para*-substituent of the arylthiolate ligand influencing the charge-transport properties.

Keywords: chain structures · S ligands · semiconductors · structure elucidation · X-ray diffraction

Introduction

Organic π-conjugated molecules and their aggregated forms have been extensively studied with regard to their charge-transport properties, which have a number of potential applications in materials science.[1] Doping electron-rich organic π-conjugated compounds with metal ions can generate diverse one-dimensional (1D) coordination solids with intriguing electronic properties.[2] According to some literature reports, conducting metal-organic wires of the second- and third-row transition metal ions are occasionally prepared by self-assembly reactions, using bifunctional bridging ligand(s) to connect the metal ions.[3] Our interest in the development of new functional metal-organic materials prompted us to investigate the structures and properties of homoleptic d^{10} metal acetylides and thiolates, which could be prepared through self-assembly reactions.[4] Homoleptic copper(I) or-

[a] Prof. C.-M. Che, Mr. C.-H. Li
Coordination Chemistry Institute
and the State Key Laboratory of Coordination Chemistry
School of Chemistry and Chemical Engineering
Nanjing University
Nanjing 210093 (P.R. China)
E-mail: cmche@hku.hk

[b] Prof. C.-M. Che, Mr. C.-H. Li, Dr. S. S.-Y. Chui, Dr. V. A. L. Roy, Mr. K.-H. Low
Department of Chemistry
and HKU-CAS Joint Laboratory on New Materials
The University of Hong Kong
Pokfulam Road, Hong Kong (China)
Fax: (+852) 2857-1586

Supporting information for this article is available on the WWW under http://www.chemeurj.org/ or from the author.

ganothiolates $[Cu(SR)]_\infty$ constitute an interesting class of electrically neutral coordination polymers, which have attracted interest in areas such as coordination chemistry,[5] materials science,[6] and as reagents for organic synthesis.[7] Extensive studies have revealed that homoleptic copper(I) organothiolates can be prepared as polynuclear $[Cu_x(SR)_y]$ clusters that may be anionic ($x=1$–8, $y=2$–12)[8] or neutral ($x=y=3$–12).[9] Polynuclear $[Cu_{13}(SCH_2CH_2NH_3)_6]^{13+}$ and $[Cu_{12}(SCH_3)_6]^{6+}$ cations have hitherto been reported.[10b,c] Neutral polymeric homoleptic $[Cu(SR)]_\infty$ compounds have been reported in the literature, but their structures remain poorly understood.[10,11] The covalency of the Cu–S bond, the bridging ability of the thiolate ligand, as well as closed-shell d^{10} cuprophilicity,[12] all contribute to the formation of $[Cu(SR)]_\infty$ polymers. In 1993, Baerlocher described the chain structure of $[Cu(SCH_3)]_\infty$, which was solved using powder X-ray diffraction data.[10a] In addition, the lamellar structures of homoleptic $[Cu(SR)]_\infty$ ($R=n$-C_xH_{2x+1}, $x=4$–18)[11b,c] and $[Cu_2(1,4\text{-}S_2C_6H_4)]_\infty$[11a] complexes had previously been proposed in the literature. Herein, we report the preparation of polycrystalline solid samples of homoleptic copper(I) arylthiolate polymers $[Cu(p\text{-}SC_6H_4\text{-}X)]_\infty$ [X = CH_3 (**1**), H (**2**), CH_3O (**3**), *t*Bu (**4**), CF_3 (**5**), NO_2 (**6**), and COOH (**7**)]. Structure determinations by powder X-ray diffraction (XRD) analysis have revealed that infinite chains of $[Cu(SR)]_\infty$ are present in polycrystalline solid samples of **1**–**3** and **6**. In contrast to the three-dimensional (3D) network of Cu_2S, the $[Cu(SR)]_\infty$ coordination polymers represent a class of 1D metal-organic semiconductors with field-effect charge mobility values of 10^{-2}–10^{-3} $cm^2V^{-1}s^{-1}$, which are comparable to those of π-conjugated oligo-[13] and polythiophene[14] compounds. The effect of the *para*-substituent of the arylthiolate ligand on the charge mobility of field-effect transistors made from nanorods of **1**–**5** and $[Cu(SCH_3)]_\infty$ is discussed.

Results and Discussion

Synthesis of $[Cu(SR)]_\infty$: The methods that have previously been used for the preparation of homoleptic $[Cu(SR)]_\infty$ polymers have been reviewed by Janssen et al.[15e] These methods include: a) synthesis by deprotonation of thiols; b) an electrochemical reaction; c) a transmetalation reaction with a Group IA metal thiolate, and d) deprotection of a trimethylsilyl thioether. Reduction of an organic disulfide under mild conditions is another possibility, which is similar to the preparation of $[Cu(SePh)]_\infty$ using diphenyl selenide.[15d] In this work, the homoleptic $[Cu(SR)]_\infty$ complexes were obtained by three methods: i) the reaction of Cu_2O with thiol ligands RSH, ii) the reaction of Cu_2O with di sulfides RSSR in the presence of a reductant ($NaBH_4$) under basic conditions, and iii) the reaction of $Cu(NO_3)_2\cdot 3H_2O$ with RSH in the presence of triethylamine. In the case of method (i), the use of an excessive amount of RSH readily led to the formation of a mixture of anionic complexes such as $[Cu(SR)_2]^-$ and $[Cu(SR)_3]^{2-}$ in alkaline solution.[8c,d] On the other hand, if Cu_2O was used in excess, the reaction product $[Cu(SR)]_\infty$ was found to be contaminated with a trace amount of Cu_2O. Using method i), when an excess of p-$NO_2C_6H_4SH$ was added to a suspension of Cu_2O in an organic solvent (EtOH, acetone, or CH_3CN), the reaction product **6** was formed, but contained a considerable amount of unreacted Cu_2O. Consequently, method ii) was used for the synthesis of **6**. Although the reactions using methods i) and ii) proceeded to completion within an hour, and the reaction products were phase-pure and obtained in moderate yields, the crystallinity of the reaction products was in all cases unsatisfactorily low, as revealed by their XRD data. Prolonged reflux (at least 48 h) was used to anneal these solid samples. We performed independent SEM and TEM studies, which revealed that the crystal morphology of the solid samples of $[Cu(SR)]_\infty$ was independent of the method of preparation. A rod-shaped crystal morphology was generally found for solid samples of **1**–**5**, whereas irregular plate-like nanocrystals were observed for **6** and **7**.

Structural descriptions of $[Cu(SR)]_\infty$: The results of structure determinations of **1**–**3** and **6** are summarized in Table 1. The structure of **1** viewed along the [100] direction is shown in Figure 1. The asymmetric unit contains two crystallographically independent copper atoms (Cu1 and Cu2) and two arylthiolate ligands. Each Cu atom displays a trigonal

Table 1. Results of structural refinements for **1**–**3** and **6**.

	1	**2**	**3**	**6**
Crystal system	monoclinic	tetragonal	monoclinic	tetragonal
space group	$P2_1/n$	$P4_2/n$	$P2_1/n$	$P4_2/n$
a [Å]	24.834(3)	17.357(2)	26.100(2)	19.727(1)
b [Å]	14.086(2)	17.357(2)	13.698(1)	19.727(1)
c [Å]	4.0298 (5)	3.826(1)	4.153(4)	3.9685(4)
α [°]	90	90	90	90
β [°]	97.99(1)	90	95.32(4)	90
γ [°]	90	90	90	90
V [Å^3]	1396.0(3)	1152.9(4)	1478.4(3)	1544.4(2)
Z	8	8	8	8
M_r	186.7	172.7	202.7	217.7
ρ_{calcd} [g cm^{-3}]	1.773	2.018	1.855	1.873
2θ range [°]	3–60	3–60	3–60	3–53
data points, $y_{i,o}$	2850	2850	2850	2500
reflections, N_{obs}	800	332	854	264
variables, N_{var}	151	83	151	92
restraints	108	46	88	43
R_p[a]	0.0493	0.0365	0.0529	0.0462
R_{wp}[a]	0.0709	0.0514	0.0746	0.0615
R_{wp} (expected)[a]	0.0409	0.0300	0.0476	0.0401
R_B[b]	0.0339	0.0331	0.1101	0.0631
goodness of fit	1.73	1.71	1.57	1.53
max. [shift/esd]^2	0.30	0.42	0.38	0.26
(mean)	(0.03)	(0.06)	(0.04)	(0.02)

[a] $R_p=\Sigma_i|y_{i,o}-y_{i,c}|/\Sigma_i|y_{i,o}|$; $R_{wp}=[\Sigma_i w_i|y_{i,o}-y_{i,c}|^2/\Sigma_i w_i|y_{i,o}|^2]^{1/2}$; expected $R_{wp}=R_{wp}/\chi^2$; $\chi^2=\Sigma_i w_i|y_{i,o}-y_{i,c}|^2/(N_{obs}-N_{var})$, where $y_{i,o}$ and $y_{i,c}$ are the observed and calculated intensities at point i of the profile, respectively; N_{obs} is the number of theoretical Bragg peaks in the 2θ range; N_{var} is number of refined parameters. Statistical weights w_i are normally taken as $1/y_{i,o}$. [b] $R_B=\Sigma|I_{j,o}-I_{j,c}|/\Sigma I_{j,o}$ (I_j denotes the extracted intensity of the j-th Bragg reflection).

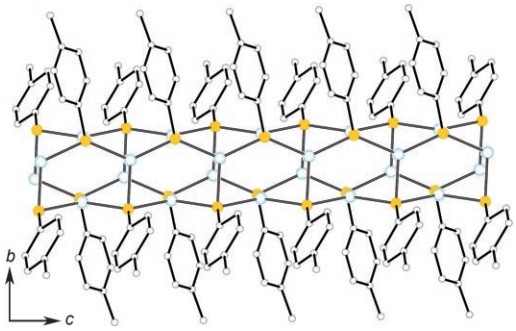

Figure 1. Perspective drawing of the chain structure of **1** viewed along the [100] direction. Note that the *p*-tolyl substituents are aligned with intra-chain π···π distances of 3.198–3.338 Å. Hydrogen atoms have been omitted for clarity.

coordination geometry (Cu1(*x*,*y*,*z*)–S2(*x*,*y*,*z*) 2.247 Å; Cu1(*x*,*y*,*z*)–S1(*x*,*y*,*z*) 2.252 Å; Cu1(*x*,*y*,*z*)–S2(*x*,*y*,*z*+1) 2.248 Å; Cu2(*x*,*y*,*z*)–S1(*x*,*y*,*z*) 2.247 Å; Cu2(*x*,*y*,*z*)–S1(*x*,*y*,*z*+1) 2.249 Å; Cu2(*x*,*y*,*z*)–S2(1−*x*,1−*y*,−*z*) 2.252 Å, with Cu-S-Cu angles of 112–127°) and is bound by three μ^3-bridging arylthiolate ligands. The structural repeating unit in **1** can be viewed as consisting of a six-membered ring with a half-chair conformation, made up of alternating linked Cu and S atoms. Each six-membered ring interconnects with two neighboring rings to form an extended ladder-like $[Cu–S]_\infty$ chain (Scheme 1). Two identical $[Cu–S]_\infty$ ladder-like chains are linked through Cu1···S1 interactions. There is a well-ordered alignment of the pendant *p*-tolyl substituents, in which the aryl rings adopt a slightly offset π-stacked configuration. The shortest distances between two mean planes of adjacent aryl rings (3.210 Å for C1–C6, 3.308 Å for C8–C14) and the closest non-bonded distances (C2(*x*,*y*,*z*)···C6(*x*,*y*,−1+*z*) 3.198 Å; C3(*x*,*y*,*z*)···C5(*x*,*y*,−1+*z*) 3.223 Å; C9(*x*,*y*,*z*)···C12(*x*,*y*,−1+*z*) 3.338 Å) are slightly less than the sum of the van der Waals radii (3.4 Å) of two carbon atoms, indicative of weak intra-chain π···π interactions. The intra-chain Cu···Cu distances are 2.923–3.132 Å, which are longer than the sum of the van der Waals radii of two Cu atoms (2.8 Å),[21] revealing the absence of cuprophilic interactions.

Complex **2**, which has an unsubstituted arylthiolate ligand, forms a chain polymer that is topologically identical to that formed by **1**. Its crystal structure possesses tetragonal symmetry, with the asymmetric unit containing one symmetry-equivalent Cu atom and one thiolate ligand. The backbone of the $[Cu(SPh)]_\infty$ chain lies along the 4_2 screw-rotation axis, resulting in S_4 symmetry of the chain. The Cu···Cu and Cu···S distances in **2** (2.956 Å and 2.270–2.303 Å, respectively) are comparable to those found in **1** and in $[Cu(SCH_3)]_\infty$ chains, indicating that there is structural resemblance among these $[Cu(SR)]_\infty$ polymers. As in the structure of **1**, there are significant intra-chain π···π stacking interactions (3.012–3.330 Å) between neighboring phenyl rings.

Complex **3** has a similar polymeric structure to those of **1** and **2**, with shorter Cu···Cu distances of 2.75–2.83 Å and longer intra-chain π···π distances (> 3.4 Å). The *p*-methoxy substituent does not appear to alter the packing of the $[Cu(SAr)]_\infty$ chains compared with that of **1** and **2**. The observed non-bonded O···H distances (2.819 Å and 3.093 Å) are considerably longer than the van der Waals distance (2.6 Å) of a typical C–H···O hydrogen bond,[22] implying insignificant inter-chain H···O interactions. The XRD pattern of **4** is given in the Supporting Information (Figure S5). There is considerable overlap of the peaks in the XRD pattern of this complex, making it difficult to derive the lattice constants by means of conventional indexing programs. We were unable to solve the structure of **4**. However, the XRD pattern of **4** reveals a low-angle diffraction peak with a large *d*-spacing of 20.5 Å, which is unique among the obtained XRD patterns of the $[Cu(SR)]_\infty$ polymers. In addition, the long repeating distance of 6.50 Å derived from the elec-

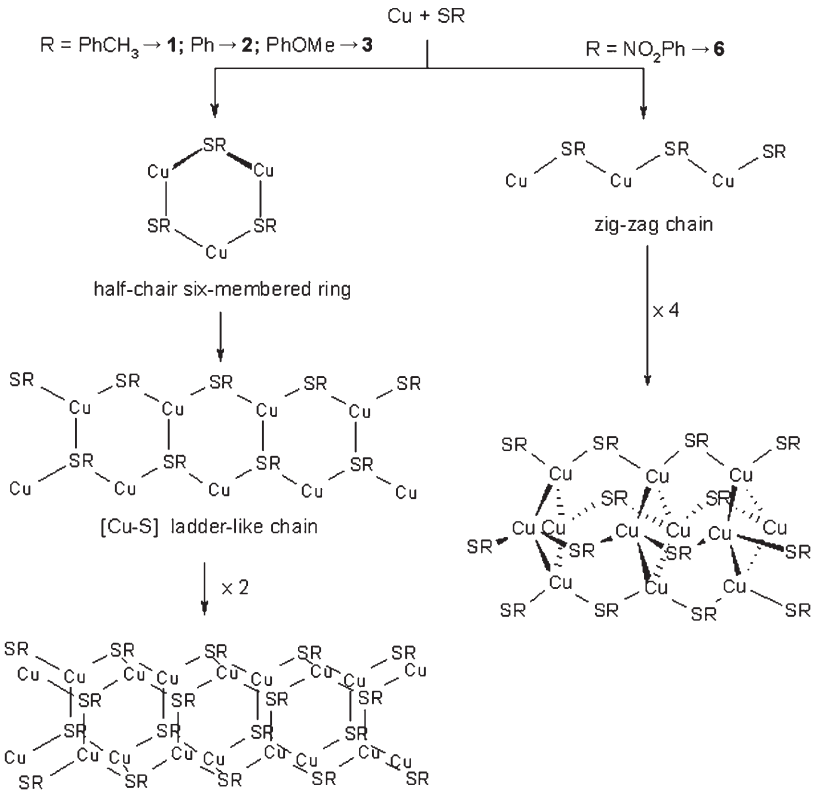

Scheme 1. Schematic diagram for the construction of **1**–**3** and **6**.

tron diffraction data reveals that **4** crystallized in a comparatively large unit cell so as to accommodate the bulky *tert*-butyl substituents. The structure of the $[Cu(SC_6H_4CF_3)]_\infty$ polymer **5** is similar to that of **2**; the powder XRD pattern (Supporting Information, Figure S5) of the former could also be indexed by a tetragonal lattice ($a=20.088$ Å and $c=3.965$ Å, $V=1599.9$ Å^3). The short c edge is consistent with the value derived from electron diffraction analysis (Supporting Information, Figure S14).

Complex **6** forms a polymeric chain structure that is significantly different from those formed by **1–3**. Presumably, the *p*-NO_2 substituent affects the structure of the polymeric chain as a result of different Cu–S connectivities. The crystal structure of **6** has the same space group as **2** ($P4_2/n$), but each thiolate S atom binds only to two Cu atoms with an average Cu···S distance of 2.35 Å, forming a zig-zag Cu–S chain (Scheme 1). The occurrence of the μ^2-bridging mode of the *p*-nitrophenylthiolate ligand may be attributed to the electron-withdrawing NO_2 substituent. As a result, the polymeric chain structure is formed by linking four identical zig-zag chains through Cu···Cu interactions (2.649 Å). Figure 2

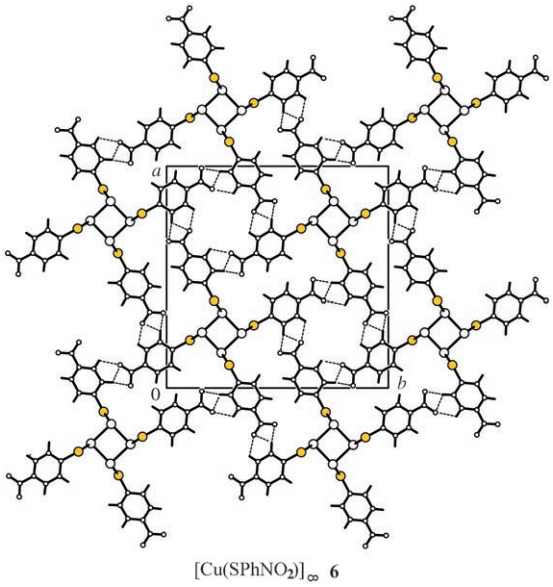

Figure 2. Crystal packing for polymer of **6**, revealing that weak interchain C–H···O–N interactions are only found in **6** (the sulfur atoms of each structure are drawn as filled circles).

depicts the packing of the polymeric chains of **6** viewed from the *c*-axis. Unlike in **1–3**, there are no significant intrachain π···π interactions ($d>3.6$ Å) in the structure of **6**, and individual $[Cu(SC_6H_4NO_2)]_\infty$ chains are predominantly held together by weak non-covalent C–H···O–N hydrogen bonds (O1(x,y,z)···H3($-\frac{1}{2}+y,1-x,\frac{1}{2}+z$) 2.586 Å; O1($x,y,z$)···C3($-\frac{1}{2}+y,1-x,\frac{1}{2}+z$) 3.217 Å; ∢O1···H3–C3 123.5°).

For the arylthiolate ligand with a *p*-COOH substituent, an insoluble pale-yellow solid $[Cu(SC_6H_4COOH)]_\infty$ (**7**) was formed. Indexing its XRD pattern gave a primitive monoclinic cell ($a=20.1051$ Å, $b=4.3766$ Å, $c=17.0505$ Å, $\beta=94.31°$, $V=1496.08$ Å^3), implying that this solid has an atomic arrangement different from those found for **1** and **3**. Based on elemental analyses and TGA data (see below), no coordinated or lattice water molecules are present in the crystal structure of **7**. This was further verified by FT-IR data, which revealed that the stretching frequencies for the O–H (3480 cm^{-1}) and C=O (1684 cm^{-1}) groups of **7** are significantly lower than those (3579 cm^{-1} and 1749 cm^{-1}) found for the free O–H groups of a self-assembled *p*-mercaptobenzoic acid monolayer deposited on a gold surface.[23] Moreover, the C–OH stretching and O–H···O bending modes observed for a solid sample of **7** are similar to those found for the free ligand in the form of a crystalline solid.

Thermal and structural stabilities: Figure 3 shows TGA curves for solid samples of **1–7** measured under an N_2 atmosphere. Irrespective of the *para*-substituent on the arylthiolate ligand, the decomposition temperatures of all of the $[Cu(SR)]_\infty$ polymers are between 200 and 300 °C, and are thus some 100 °C higher than that found for the aliphatic $[Cu(SCH_3)]_\infty$ analogue. For **1–7** (with the exception of **5**), an initial weight loss of about 40–55 % at around 250–370 °C was noted, which could be attributed to dearomatization of the arylthiolate ligand in each case. A polycrystalline sample of **5** displayed two consecutive weight losses of 45 % and 17 % near 240 and 310 °C, respectively. The former process is attributed to degradation of the arylthiolate ligand, as was observed for **1–4**, whereas the latter weight loss corresponds to the release of two molar equivalents of HF. Slightly larger initial weight losses were noted for solid samples of **6** and **7**, which could be attributed to the production of NO_2 and CO_2, respectively. Upon heating above 400 °C, all of the $[Cu(SR)]_\infty$ polymers **1–7** underwent an additional

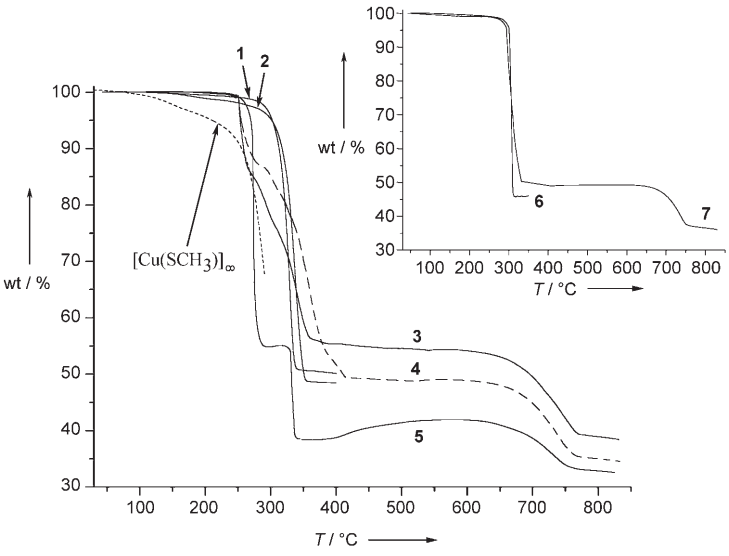

Figure 3. TGA curves for solid samples of **1–5** and $[Cu(SCH_3)]_\infty$ (-----) under N_2. TGA curves for solid samples of **6** and **7** are shown in the inset.

15–19% weight loss, which was consistent with the release of one molar equivalent of H_2S. The powder XRD patterns of the carbonaceous residues revealed that they were composed of complicated solid mixtures of CuO (tenorite (PDF-2 05-0661)), Cu_2O (cuprite (PDF-2 05-0667)), and Cu_2S (chalcocite-M (PDF-2 033–0490) and djurleite (PDF-2 034-0660)). In situ variable-temperature X-ray diffractometry measurements in the temperature range 30–300°C were performed to determine the stabilities of the polymeric chain structures of **1**–**7**. Powder XRD patterns of solid samples of **1**, **7**, and $[Cu(SCH_3)]_\infty$, collected at temperatures from 30°C to 300°C, are given in the Supporting Information (Figures S7–S9). We found **7** to be slightly more stable than **1** or $[Cu(SCH_3)]_\infty$. The chain structure of **1** slowly degraded over the temperature range 30–150°C, and rapidly lost its structural integrity at temperatures above 175°C. The $[Cu(SCH_3)]_\infty$ polymer was found to be slightly less stable under identical experimental conditions.

TEM and SAED studies: Figure 4 shows a transmission electron microscopy (TEM) image and a selected-area electron diffraction (SAED) pattern of a polycrystalline solid sample of **1**. This solid sample contained homogeneously dispersed nanorods, which were a few micrometers long with an average width of 30–60 nm, and which formed extensive lateral aggregations. Interestingly, the SAED pattern of an individual nanorod revealed parallel rows of sharp diffraction spots that could be roughly indexed by the lattice parameters derived from the aforementioned powder XRD data. Notably, the short crystallographic *c*-axis of **1** is roughly parallel to the long axis of the nanorod. Similar rod-like crystal morphologies and SAED patterns were observed for **2**–**5** and $[Cu(SCH_3)]_\infty$ (Supporting Information, Figures S10–S14). From the shorter *c*-axes of their SAED patterns, the calculated interplanar *d*-spacings for **1**–**5** (except **4**) and $[Cu(SCH_3)]_\infty$ are comparable to the short crystallographic axes of their crystal structures. The nanorods of **2**–**5** and $[Cu(SCH_3)]_\infty$ with lengths of several micrometers were found to have variable widths in the range 20–250 nm (50–100 nm for **2**, 50–100 nm for **3**, 50–80 nm for **4**, 20–60 nm for **5**, and 50–250 nm for $[Cu(SCH_3)]_\infty$, respectively). On the other hand, polycrystalline solid samples of **6** and **7** formed irregularly shaped plate-like nanocrystals. The SAED pattern of the plate-like nanocrystals of **6** (Figure 5) revealed weak concentric diffraction rings, indicating that the $[Cu(SC_6H_4NO_2)]_\infty$ chains were randomly oriented. A similar SAED pattern for the nanocrystals of **7** (Supporting Information, Figure S15) indicated a similar arrangement.

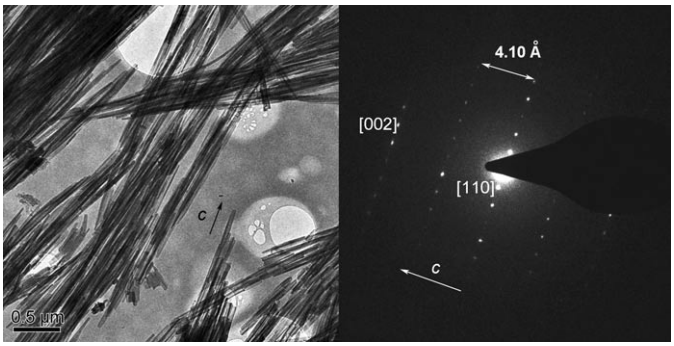

Figure 4. TEM image (5000×) (left) and SAED pattern (right) of nanorods of **1**. Scale bar left: 0.5 μm.

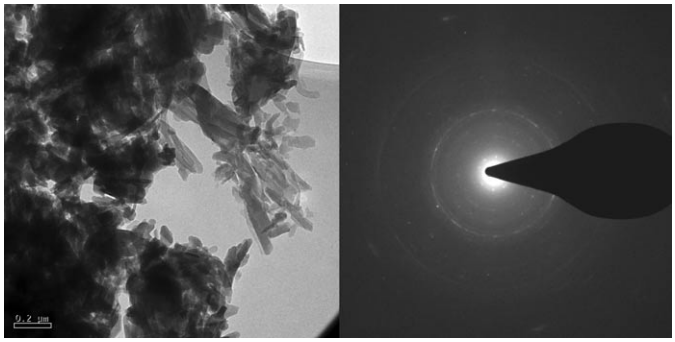

Figure 5. TEM image (12500×) (left) and SAED pattern (right) of nanocrystals of **6**. Scale bar left: 0.2 μm.

Charge mobilities of nanorod FET devices: Preliminary four-point probe electrical measurements suggested that a pellet sample made from a polycrystalline solid sample of **1** had a bulk resistivity of about 800 Ω cm at room temperature. This value is lower than that of Cu_2O (1000–5000 Ω cm), but significantly higher than that of Cu_2S (0.008–0.010 Ω cm).[24] Bottom-contact field-effect transistors (FETs) were fabricated by drop-casting methanolic suspensions of polycrystalline solid samples of **1**–**7** on top of patterned SiO_2 substrates; the charge mobility measurements were subsequently performed under a nitrogen atmosphere in a glove box. Figure 6 shows the output (I_{DS} versus V_{GS} at different V_{DS}) and transfer (I_{DS} versus V_{GS} at $V_{DS} = -10$ V) characteristics of a device made from nanorods of **1**. When operated in accumulation mode, the drain-source current I_{DS} increased with the negative gate voltages V_{DS} and V_{GS}, indicative of p-type FET behavior. However, the channel was found to be open, even at $V_{GS} = 0$ V, probably due to bulk conduction of the nanorods between the source and drain electrodes. Since saturation of I_{DS} had not been attained, the charge mobility μ was calculated in the linear regime,[16] where $V_{DS} \ll V_{GS}$. We found that the charge mobilities, μ, of the devices made from nanorods of **1**–**3**, 7.0×10^{-2} $cm^2V^{-1}s^{-1}$ for **1**, 6.2×10^{-3} $cm^2V^{-1}s^{-1}$ for **2**, and 1×10^{-2} $cm^2V^{-1}s^{-1}$ for **3**, were 10^4 and 10^5 times higher than those of devices made from **4** and **5**, respectively. A device made from nanorods of $[Cu(SCH_3)]_\infty$ also exhibited a charge mobility of 6×10^{-2} $cm^2V^{-1}s^{-1}$. This suggests that the charge transportation originates from the 1D $[Cu{-}S]_\infty$ network. In addition, the devices made from nanorods of **1**–**4** (widths ~30–60 nm) were robust as the charge mobility values of these devices after storing them inside a glove box under a nitrogen atmosphere for several months were almost identical to the initial values. The devices made from

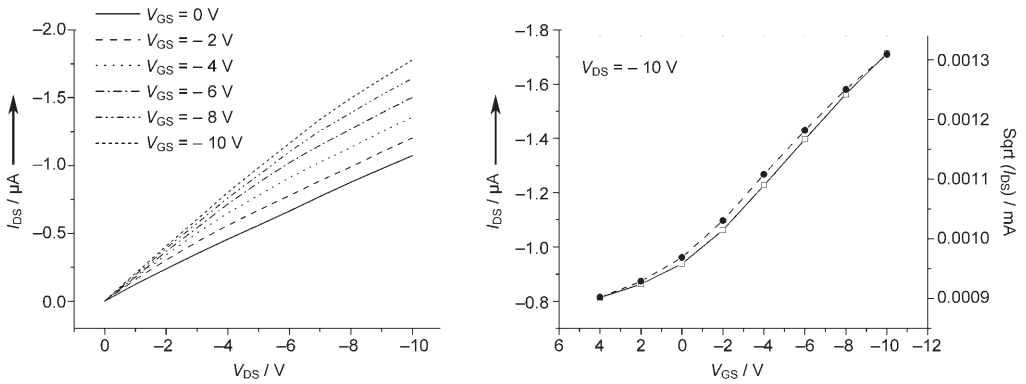

Figure 6. Output (left) and transfer (right) characteristics of the FET device fabricated with nanorods of **1**.

plate-like nanocrystals of **6** and **7** displayed negligible μ values ($<10^{-6}$ cm^2 V^{-1} s^{-1}) under the same experimental conditions.

Diffuse reflectance spectra: As described by Tauc,[25a] the absorption coefficient, α, and the optical band gap of a thin layer of a solid sample are related by the expression $\alpha h\nu = A(h\nu - E_g)^r$, where $h\nu$ is the photon energy, A is a constant, E_g is the optical energy gap, and r is characteristic of the type of optical transition process, having values of 0.5 and 2 for direct allowed and indirect allowed optical transitions, respectively.[25b] The absorption coefficient can also be written in terms of reflectance as $\alpha = B\{\ln[(R_{max}-R_{min})/(R-R_{min})]\}$, where B is a parameter related to the thickness of the sample.[25c] By plotting $\{h\nu \ln[(R_{max}-R_{min})/(R-R_{min})]\}^2$ against $h\nu$ and extrapolating the linear region of the curve, E_g could be obtained at $\alpha = 0$. Figure 7 shows the relationships between the absorption coefficients, α, derived from solid-state diffuse reflectance spectra of **1**–**7** and $[Cu(SCH_3)]_\infty$ and the photon energies measured from 250 nm to 1100 nm (or 4.95 eV to 1.13 eV). The results of optical band gap determinations are given in the Supporting Information (Figures S16–S23). Polycrystalline samples of **1**–**4** and $[Cu(SCH_3)]_\infty$ each exhibited optical absorptions with λ_{max} at 463–492 nm, revealing that the optical band gaps of these complexes are between 2.52 eV and 2.68 eV. For **5** and **6** with electron-withdrawing substituents on the arylthiolate ligands, smaller band gaps were observed (1.97 eV and 2.23 eV, respectively). The optical band gap of **7** was found to be 2.96 eV; the deviation from the trend depicted in Figure 7 may originate from the different chain structure of **7** compared to those of **5** and **6** as a consequence of the intermolecular hydrogen bonding present in the crystalline sample.

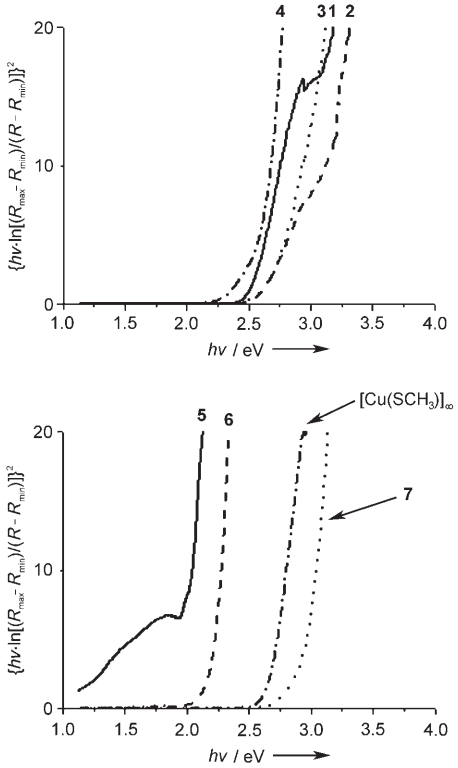

Figure 7. Plots of $\{h\nu \ln[(R_{max}-R_{min})/(R-R_{min})]\}^2$ against $h\nu$ for solids **1**–**7** and $[Cu(SCH_3)]_\infty$. Optical band gaps [eV] were obtained by extrapolation of the linear region onto the x-axis: (2.52 for **1**, 2.59 for **2**, 2.68 for **3**, 2.62 for **4**, 1.97 for **5**, 2.23 for **6**, 2.96 for **7**, and 2.67 for $[Cu(SCH_3)]_\infty$).

Discussion

Over the past few decades, metal-organic complexes of third-row transition metal ions such as Os^{II}, Ir^{III}, Pt^{II}, and Au^{I} have been extensively studied with regard to their use in organic light-emitting diode devices.[26] However, there have been only a few reports on the applications of first-row transition metal complexes in organic optoelectronics.[26e] While π-conjugated organic molecules such as pentacenes[27] and oligothiophenes[13,14] have been extensively studied for the fabrication of field-effect transistors (FETs), related work involving metal-organic complexes has been sparse. Notably, however, copper(II) phthalocyanines have been extensively studied in relation to FETs, and relatively high charge mobility values (0.01–0.02 cm^2 V^{-1} s^{-1}) have been attained.[28] Compared with π-conjugated organic materials,

the $[Cu(SR)]_\infty$ polymers described in this work are inexpensive and easily prepared in high yields and purities; these are advantages for developing applications of $[Cu(SR)]_\infty$ in materials science. We have found that the charge mobilities of nanorod FETs fabricated from $[Cu(SR)]_\infty$ polymers cover a wide range of values (10^{-2}–10^{-5} $cm^2V^{-1}s^{-1}$) and are thus comparable to those of 10^{-2} $cm^2V^{-1}s^{-1}$ reported for oligothiophene[13] and polythiophene compounds.[14]

For π-conjugated organic materials, weak cofacial π···π stacking interactions play a key role in the charge-transport properties of the as-fabricated organic FETs.[29] In this work, the charge-transport behavior of the $[Cu(SR)]_\infty$ polymers was found to show no direct correlation with either π···π interactions, as in the cases of **1**–**3**, or with the electronic effect of the arylthiolate ligand, as in the cases of **5**–**7**. In view of the finding that nanorod transistors made from **1** and $[Cu(SCH_3)]_\infty$ have comparable charge mobility values, we propose that the charge conduction pathway originates from an intrinsic hopping mechanism[30] within the covalently bound $[Cu–S]_\infty$ chain network. In the literature, two models, namely trapping-release[31] and phonon-assisted tunneling hopping transport,[32] combined with the Gaussian disorder representation,[33] have been proposed to account for the observed field-dependent mobility in organic FETs operating in the accumulation mode. The trapping-release model is based on the assumption that most of the charge carriers are trapped within localized states in a solid sample and that the amount of charge carriers released into the extended-state transport level(s) depends on the energy level(s) of the localized states, the temperature, and the gate voltage. Extended-state transport can only occur in materials with a highly ordered structure. The charge carriers in an amorphous solid sample are strongly localized, and consequently this usually leads to poor mobility. In this regard, charge injection and transport within the copper–sulfur networks of **1**–**4** and $[Cu(SCH_3)]_\infty$ are likely to originate from the well-ordered atomic arrangements in their 1D polymeric structures. The charge-transport mechanism operating in the polymeric chain structures of $[Cu(SR)]_\infty$ may be different from those found in other Cu-containing polymers such as $[Cu^I(TANC)F_{0.5}]_\infty$ (TANC = 5,6,11,12-tetraazanaphthacene) and $[Cu(N_2C_2S_2)]_\infty$ ($N_2C_2S_2$ = dithiooxamide dianion) that have previously been reported in the literature, in which disordered interstitial fluoride ions[34] or an iodine dopant[35] were involved in charge transportation, respectively. In this work, we have shown that both the *para*-substituent of the arylthiolate ligand and the crystal morphology influence the overall charge mobility. The presence of an electron-donating substituent such as CH_3 or CH_3O, as in the cases of **1** and **3**, leads to an increase in the charge mobility from 10^{-3} $cm^2V^{-1}s^{-1}$ to 10^{-2} $cm^2V^{-1}s^{-1}$. This is attributed to the stabilization of p-type charge carriers within the nanorods. Assuming that the chain structure of **4** is similar to those of **1**–**3**, the bulky *tert*-butyl substituents in **4** would increase the average interchain separation, making charge-hopping between adjacent polymer chains less efficient, and consequently leading to reduced charge mobility. Nanorods of **5** have an average crystalline size that is comparable to those of nanorods of **1**–**4**, but were found to display a significantly lower charge mobility. It is possible that the electron-withdrawing CF_3 substituent destabilizes the positively charged carriers and hence disfavors charge injection and transport. The effects of peripheral and end substituent groups on the charge-transport behavior of pentacene compounds have previously been investigated. Di- and tetrasubstituted pentacene compounds generally show p-type charge mobilities,[36a,c] whereas electron-deficient perfluorinated pentacene behaves as an n-type material with an electron mobility of 0.11 $cm^2V^{-1}s^{-1}$.[36b] Compared to the nanorods present in polycrystalline solid samples of **1**–**5**, a polycrystalline solid sample of $[Cu(SCH_3)]_\infty$ was found to contain comparatively wide nanorods, leading to larger grain sizes, which may account for its high charge mobility of 6×10^{-2} $cm^2V^{-1}s^{-1}$. It can also be argued that charge transport in a polycrystalline material may be limited by grain boundaries, so that when the grain size is increased the number of grain boundaries decreases, leading to better charge transport. This situation has previously been reported for oligothiophenes.[37] However, the opposite relationship was found for pentacene compounds.[38] The plate-like crystal morphologies of crystalline solid samples of **6** and **7** reveal that the $[Cu(SR)]_\infty$ chains of these two complexes adopt an orientation that would not favor efficient charge transport. For these $[Cu(SR)]_\infty$ chains, their spatial orientation may be modulated by weak interactions associated with the peripheral NO_2 or COOH substituents. Although we have not been able to determine the crystal structure of **7**, we suggest that the Cu^I atoms of the $[Cu(SC_6H_4COOH)]_\infty$ polymer are connected by μ^2-bridges formed by the S atoms of the arylthiolate ligands, and that inter-chain hydrogen-bonding interactions between the carboxylic acid groups lead to aggregation. A recent study has revealed that the charge-transport properties of thin-film field-effect transistors fabricated from perylo[1,12-*b*,*c*,*d*]thiophene also exhibited a strong dependence on the film quality and morphology as well as on the packing of the molecules.[39]

We propose that the different crystal morphologies (nanorod versus plate-like) of the $[Cu(SR)]_\infty$ polymers are due to different anisotropic crystal growth rates.[40a] Scheme 2 shows the proposed modes of crystal growth of **1**–**7**, which are presumably affected by a subtle balance of intra-/interchain interactions. It has previously been found that the size of a crystal face is inversely proportional to the rate of crystal growth in the direction perpendicular to it.[40b] For solids **1**–**5** and $[Cu(SCH_3)]_\infty$, 1D crystal growth may occur preferentially along the chain axis, because the Cu atoms and SR ligands associate more rapidly to form a chain, driven by strong covalent Cu···S bonding. Weak intra-chain π···π interaction(s) may also contribute to this process, as may be the case with **1**–**3**. Whenever these adhesive forces are weakened, interchain interactions, such as C–H···O–N or O···H···O hydrogen-bonding interactions, will facilitate crystal growth in a direction perpendicular to the chain axis, leading to a plate-like morphology, as has been found with **6**

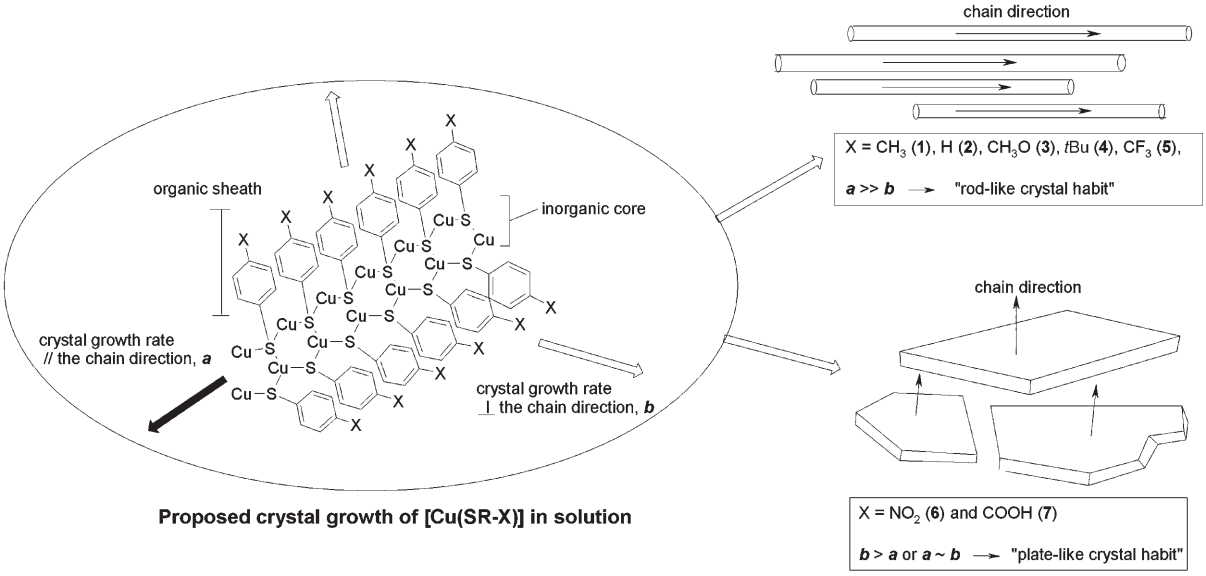

Scheme 2. Schematic drawing showing the formation of crystalline solids of **1**–**7** having distinct crystal morphologies (nanorod versus plate-like) as a consequence of different crystal growth rates in two orthogonal directions.

and **7**. For nanocrystals of **6** and **7**, the dipole moment of the arylthiolate ligands may also affect the crystal morphology.

Conclusion

In summary, we have developed a high-yielding synthesis for the production of phase-pure polycrystalline solid samples of $[Cu(SR)]_\infty$ polymers. These polymers were subsequently used for the fabrication of nanorod FETs, all of which exhibited a p-type charge mobility with μ values of 10^{-2}–$10^{-5}\,cm^2\,V^{-1}\,s^{-1}$. The performances of nanorod FETs made from these homoleptic $[Cu(SR)]_\infty$ polymers have been found to be significantly affected by the *para*-substituent of the arylthiolate ligand. The crystal morphologies of the polymeric $[Cu(SR)]_\infty$ chains are affected by weak intra- and interchain interactions.

Experimental Section

Polycrystalline solid samples of **1**–**7** were prepared according to a previously described literature method.[15] The copper source was either Cu_2O or a Cu^{II} salt in the presence of a reducing agent ($NaBH_4$). All reaction products were obtained as phase-pure polycrystalline solids, which were air-stable and insoluble in most common organic solvents. Elemental analyses of **1**–**7** were performed at the Institute of Chemistry, Chinese Academy of Science; the metal/ligand ratios were found to be 1:1.

[Cu(*p*-SC$_6$H$_4$-X)] (X = CH$_3$ (1), H (2)): *p*-Tolyl disulfide (0.565 g, 2.3 mmol) or phenyl disulfide (0.502 g, 2.3 mmol) was added to a solution of NaOH (0.093 g, 2.3 mmol) in water (30 mL), and then a solution of $NaBH_4$ (0.087 g, 2.3 mmol) in methanol (30 mL) was added. The yellow suspension was heated until a clear solution was obtained. After cooling to room temperature, the solution was adjusted to pH ≈ 5–6 by the dropwise addition of concentrated hydrochloric acid (12 M). Cu_2O (0.288 g, 2 mmol) was then added with stirring and the reaction mixture was refluxed for 72 h. The insoluble yellow precipitate was collected by filtration, and washed with water, methanol, acetone, dichloromethane, and diethyl ether. Yields: 89% (0.67 g) for **1** and 85% (0.59 g) for **2**; elemental analysis calcd (%) for **1**: C 45.02, H 3.78; found: C 44.95, H 3.69; calcd (%) for **2**: C 41.72, H 2.92; found: C 41.39, H 2.82.

[Cu(*p*-SC$_6$H$_4$-X)] (X = CH$_3$O (3), *t*Bu (4), CF$_3$ (5), and COOH (7)): For **3**, Cu_2O (0.500 g, 3.5 mmol) was added to a stirred solution of 4-methoxybenzenethiol (0.980 g, 7.0 mmol) in ethanol (50 mL) and the mixture was refluxed for 12 h. For **4**, **5**, and **7**, 4-(*tert*-butyl)benzenethiol (1.162 g, 7.0 mmol), 4-(trifluoromethyl)benzenethiol (1.245 g, 7.0 mmol), and 4-mercaptobenzoic acid (1.078 g, 7.0 mmol) were used, respectively. For **5** and **7**, the reaction time was extended to 48 h. The resulting yellow suspensions were filtered, and the collected solids were washed with ethanol and diethyl ether, and then dried at 70 °C under a vacuum of 10 mmHg for 12 h. Yields: 90% (1.273 g) for **3**, 82% (1.312 g) for **4**, 77% (1.301 g) for **5**, and 82% (1.236 g) for **7**; elemental analysis calcd (%) for **3**: C 41.47, H 3.48; found: C 41.25, H 3.48; calcd (%) for **4**: C 52.49, H 5.73; found: C 51.93, H 5.72; calcd (%) for **5**: C 34.93, H 1.67; found: C 34.43, H 1.74; calcd (%) for **7**: C 38.79, H 2.33; found: C 37.72, H 2.38.

[Cu(*p*-SC$_6$H$_4$-X)] (X = NO$_2$ (6)): $Cu(NO_3)_2{\cdot}3H_2O$ (0.242 g, 1 mmol) was added to a solution of 4-nitrobenzenethiol (0.170 g, 1.1 mmol) and triethylamine (0.110 g, 1.1 mmol) in ethanol (30 mL). An orange precipitate was formed immediately. The resulting suspension was refluxed for 48 h. The insoluble orange solid was collected by filtration and washed with water, ethanol, acetone, dichloromethane, and diethyl ether. Yield: 95% (0.207 g); elemental analysis calcd (%) for **3**: C 33.10, H 1.85, N 6.43; found: C 33.52, H 1.85, N 6.52. We found that an orange solid, presumed to be $[Cu(SC_6H_4NO_2)]_\infty$, obtained from the reaction of Cu_2O with $HSC_6H_4NO_2$, had a high degree of crystallinity but contained a trace amount of unreacted Cu_2O.

[Cu(SCH$_3$)]$_\infty$: Cu_2O (0.289 g, 2 mmol) was added to a solution of $NaSCH_3$ (0.162 g, 2.3 mmol) in water (30 mL). The resulting brownish-red suspension was refluxed and a light-yellow solid was formed after 48 h. This insoluble yellow solid was collected by filtration and washed with water, methanol, acetone, dichloromethane, and diethyl ether. Yield: 95% (0.210 g); elemental analysis calcd (%) for $[Cu(SCH_3)]_\infty$: C 10.86, H 2.73; found: C 10.78, H 2.69.

Physical characterization: Thermogravimetric analyses were performed under an N_2 atmosphere using a Perkin-Elmer TGA-7 apparatus. In situ variable-temperature X-ray diffractograms were recorded using a Bruker D8 Advance diffractometer equipped with a modular temperature cham-

ber attachment (Materials Research Instruments) operating in the temperature range 25–450 °C. TEM images and SAED patterns were recorded using a Philips Tecnai 20 system. A few drops of an ethanolic suspension of a solid sample of **1**–**7** or $[Cu(SCH_3)]_\infty$ were placed on a copper grid for TEM and SAED experiments. A preliminary four-point conductivity measurement using a pellet sample of **1** was performed using a colinear probe system (Keithley Instruments, Inc., Model 6221). Diffuse reflectance spectra of solid samples of **1**–**7** and $[Cu(SCH_3)]_\infty$ were recorded using a Perkin-Elmer Lambda 20 UV/Vis spectrophotometer over the wavelength range 250–1100 nm. The sample was placed against a white background plate for data collection. FT-IR spectra were collected using a Bio-Rad spectrophotometer over the range 400–4000 cm^{-1}.

Field-effect transistors and charge mobility measurements: A typical substrate-gate structure field-effect transistor was fabricated. A gate oxide SiO_2 layer (100 nm, relative permittivity = 3.9) was grown thermally on a heavily doped n-type Si substrate (gate electrode). An image reversal photolithography technique was used to etch the photoresist layer and to form the source and drain pattern on the gate oxide. Source and drain metal layers, consisting of a Ti adhesion film (10 nm, lower) and an Au conductive film (50 nm, upper), were deposited by thermal evaporation. After deposition of the metal films, a standard lift-off process involving washing with acetone was used to remove the uncovered photoresist materials, leaving behind the Ti/Au source/drain contact patterns. The channel length and width of the devices were 100 μm and 1000 μm, respectively. Methanolic suspensions of **1**–**7** or $[Cu(SCH_3)]_\infty$ were each ultrasonicated for more than 12 h to fully disperse the nanorods. The respective dispersed nanorods were then drop-cast on the top of the patterned bottom-contact field-effect transistors. When transistors were made from suspensions that had not been ultrasonicated, considerable amounts of highly aggregated nanorods were found, and this enhanced aggregation led to supersaturated current–voltage behavior with a high channel current and p-type behavior, probably due to bulk conduction between the source and drain electrodes. The transistor output and transfer characteristics were measured with a probe station under nitrogen atmosphere using a Keithley K4200 semiconductor parameter analyzer. Although non-saturating behavior was found for these nanorod FET devices, a clear gate effect on the current was observed, as depicted in Figure 6. Since saturation of the drain current was not attained, the charge-carrier mobility was extracted from the linear regime of the $I_{D,lin}$ versus V_{GS} plot.[16] In the linear regime where $V_{DS} \ll V_{GS}$,

$$\mu = \frac{\partial I_{ds}/\partial V_{gs} L}{W C_{ox} V_d}$$

where W is the channel width, L is the channel length, C_{ox} is the capacitance of the SiO_2 insulating layer, V_{GS} is the gate voltage, and V_d is the drain-source voltage.

Structure determination: The structures of **1**–**3** and **6** were solved using powder X-ray diffraction data; the details are given in the Supporting Information. The unit cell parameters were determined using the indexing programs TREOR90[17a] and DICVOL04[17b] and were subsequently refined using Pawley's fitting.[18] Initial positions of the heavy atoms (Cu and S) were obtained by global optimization of the diffraction patterns using a simulated annealing algorithm implemented in the structure solution program DASH[19a] (or parallel tempering in FOX).[19b] Partial structure solutions were gradually completed by adding the missing atoms of the arylthiolate ligands. Structural refinement was performed using the GSAS/EXPGUI program suite.[20] The final cycles of the refinements of **1**–**3** and **6** are depicted as plots in the Supporting Information (Figures S1–S4). Crystallographic data (excluding structure factors) for the structures of **1**–**3** and **6** are summarized in Table 1.

CCDC-621718 (**1**), 621719 (**2**), 621720 (**3**), and 621721 (**6**) contain the supplementary crystallographic data for this paper. These data can be obtained free of charge from The Cambridge Crystallographic Data Centre via www.ccdc.cam.ac.uk/data_request/cif.

Acknowledgements

We acknowledge support from the University Development Fund (UDF), the Strategic Research Themes on Organic Optoelectronics and Nanobiotechnology of The University of Hong Kong, and the National Natural Science Foundation of China/Research Grants Council Joint Research Scheme [N_HKU 742/04]. S.S.Y.C. acknowledges the award of a postdoctoral fellowship from The University of Hong Kong. Mr. Frankie Chan from the Electron Microscope Unit (EMU) of HKU is acknowledged for technical assistance in performing the TEM and SAED experiments. We thank for Dr. Rory Watt for his help in editing this manuscript.

[1] a) J. H. Perlstein, *Angew. Chem.* **1977**, *89*, 534–549; *Angew. Chem. Int. Ed. Engl.* **1977**, *16*, 519–534; b) J. M. Williams, A. J. Schultz, U. Ceiser, K. D. Carlson, U. Geiser, H. H. Wang, A. M. Kini, M. H. Whangbo, *Organic Superconductors (including Fullerenes)*, Prentice Hall, Englewood Cliffs, NJ, **1992**; c) A. G. MacDiarmid, *Angew. Chem.* **2001**, *113*, 2649–2659; *Angew. Chem. Int. Ed.* **2001**, *40*, 2581–2590; d) A. J. Heeger, *Angew. Chem.* **2001**, *113*, 2660–2682; *Angew. Chem. Int. Ed.* **2001**, *40*, 2591–2611; e) A. N. Aleshin, *Adv. Mater.* **2006**, *18*, 17–27; f) H. Klauk, *Organic Electronics, Materials, Manufacturing and Applications*, Wiley-VCH, Weinheim, **2006**.

[2] a) C. T. Chen, K. S. Suslick, *Coord. Chem. Rev.* **1993**, *128*, 293–322; b) P. Nguyen, P. Gómez-Elipe, I. Manners, *Chem. Rev.* **1999**, *99*, 1515–1548; c) C. Janiak, *Dalton Trans.* **2003**, 2781–2804; d) I. Manners, *Synthetic Metal-Containing Polymers*, Wiley-VCH, Weinheim, Germany, **2004**.

[3] a) J. P. Collman, J. T. McDevitt, G. T. Yee, C. R. Leidner, L. G. McCullough, W. A. Little, J. B. Torrance, *Proc. Natl. Acad. Sci.* USA **1986**, *83*, 4581–4585; b) A. Aumüller, P. Erk, G. Klebe, S. Hünig, J. U. von Schütz, H. P. Werner, *Angew. Chem.* **1986**, *98*, 759–761; *Angew. Chem. Int. Ed. Engl.* **1986**, *25*, 740–741; c) R. Kato, H. Kobayashi, A. Kobayashi, *J. Am. Chem. Soc.* **1989**, *111*, 5224–5232; d) K. Sinzger, S. Hünig, M. Jopp, D. Bauer, W. Bietsch, J. U. von Schütz, H. C. Wolf, R. K. Kremer, T. Metzenthin, *J. Am. Chem. Soc.* **1993**, *115*, 7696–7705; e) G. M. Finniss, E. Canadell, C. Campana, K. R. Dunbar, *Angew. Chem.* **1996**, *108*, 2946–2948; *Angew. Chem. Int. Ed. Engl.* **1996**, *35*, 2772–2774; f) R. A. Heintz, H. Zhao, X. Ouyang, G. Grandinetti, J. Cowen, K. R. Dunbar, *Inorg. Chem.* **1999**, *38*, 144–156; g) M. Munakata, G. L. Ning, Y. Suenaga, T. Kuroda-Sowa, M. Maekawa, T. Ohta, *Angew. Chem.* **2000**, *112*, 4729–4731; *Angew. Chem. Int. Ed.* **2000**, *39*, 4555–4557; h) F. A. Cotton, E. V. Dikarev, M. A. Petrukhina, *J. Organomet. Chem.* **2000**, *596*, 130–135; i) E. Solari, J. Hesschenbrouck, R. Scopelliti, C. Floriani, N. Re, *Angew. Chem.* **2001**, *113*, 958–960; *Angew. Chem. Int. Ed.* **2001**, *40*, 932–934; j) K. Sakai, E. Ishigami, Y. Konno, T. Kajiwara, T. Ito, *J. Am. Chem. Soc.* **2002**, *124*, 12088–12089; k) M. Mitsumi, K. Kitamura, A. Morinaga, Y. Ozawa, M. Kobayashi, K. Toriumi, Y. Iso, H. Kitagawa, T. Mitami, *Angew. Chem.* **2002**, *114*, 2891–2895; *Angew. Chem. Int. Ed.* **2002**, *41*, 2767–2771; l) S. Q. Liu, T. Kuroda-Sowa, H. Konaka, Y. Suenaga, M. Maekawa, T. Mizutani, G. L. Ning, M. Munakata, *Inorg. Chem.* **2005**, *44*, 1031–1036; m) M. Mitsumi, H. Goto, S. Umebayashi, Y. Ozawa, M. Kobayashi, T. Yokoyama, H. Tanaka, S. Kuroda, K. Toriumi, *Angew. Chem.* **2005**, *117*, 4236–4240; *Angew. Chem. Int. Ed.* **2005**, *44*, 4164–4168; n) K. Otsubo, A. Kobayashi, H. Kitagawa, M. Hedo, Y. Uwatoko, H. Sagayama, Y. Wakabayashi, H. Sawa, *J. Am. Chem. Soc.* **2006**, *128*, 8140–8141.

[4] a) S. S. Y. Chui, M. F. Y. Ng, C. M. Che, *Chem. Eur. J.* **2005**, *11*, 1739–1749; b) S. S. Y. Chui, R. Chen, C. M. Che, *Angew. Chem.* **2006**, *118*, 1651–1654; *Angew. Chem. Int. Ed.* **2006**, *45*, 1621–1624.

[5] a) I. G. Dance, *Polyhedron* **1986**, *5*, 1037–1104; b) B. Krebs, G. Henkel, *Angew. Chem.* **1991**, *103*, 785–804; *Angew. Chem. Int. Ed. Engl.* **1991**, *30*, 769–788.

[6] a) T. H. Larsen, M. Sigman, A. Ghezelbash, R. C. Doty, B. A. Korgel, *J. Am. Chem. Soc.* **2003**, *125*, 5638–5639; b) M. B. Sigman, Jr., A. Ghezelbash, T. Hanrath, A. E. Saunders, F. Lee, B. A.

Korgel, *J. Am. Chem. Soc.* **2003**, *125*, 16050–16057; c) L. Chen, Y. B. Chen, L. M. Wu, *J. Am. Chem. Soc.* **2004**, *126*, 16334–16335; d) S. Schneider, Y. Yang, T. J. Marks, *Chem. Mater.* **2005**, *17*, 4286–4288; e) S. Schneider, J. A. S. Roberts, M. R. Salata, T. J. Marks, *Angew. Chem.* **2006**, *118*, 1765–1768; *Angew. Chem. Int. Ed.* **2006**, *45*, 1733–1736.

[7] a) D. M. Knotter, D. M. Grove, W. J. J. Smeets, A. L. Spek, G. van Koten, *J. Am. Chem. Soc.* **1992**, *114*, 3400–3410; b) A. Haubrich, M. van Klaveren, G. van Koten, G. Handke, N. Krause, *J. Org. Chem.* **1993**, *58*, 5849–5852; c) M. van Klaveren, F. Lambert, D. J. F. M. Eijkelkamp, D. M. Grove, G. van Koten, *Tetrahedron Lett.* **1994**, *35*, 6135–6138; d) E. S. M. Persson, M. van Klaveren, D. M. Grove, J. E. Bäckvall, G. van Koten, *Chem. Eur. J.* **1995**, *1*, 351–359; e) M. van Klaveren, E. S. M. Persson, A. del Villar, D. M. Grove, J. E. Bäckvall, G. van Koten, *Tetrahedron Lett.* **1995**, *36*, 3059–3062.

[8] a) I. G. Dance, *J. Chem. Soc. Chem. Commun.* **1976**, 68–69; b) F. J. Hollander, D. Coucouvanis, *J. Am. Chem. Soc.* **1977**, *99*, 6268–6280; c) D. Coucouvanis, C. N. Murphy, S. K. Kanodia, *Inorg. Chem.* **1980**, *19*, 2993–2998; d) C. D. Garner, J. R. Nicholson, W. Clegg, *Inorg. Chem.* **1984**, *23*, 2148–2150; e) J. R. Nicholson, I. L. Abrahams, W. Clegg, C. D. Garner, *Inorg. Chem.* **1985**, *24*, 1092–1096; f) M. Baumgartner, H. Schmalle, E. Dubler, *Polyhedron* **1990**, *9*, 1155–1164; g) K. Fujisawa, S. Imai, N. Kitajima, Y. Moro-oka, *Inorg. Chem.* **1998**, *37*, 168–169.

[9] a) Q. C. Yang, K. Tang, H. Liao, Y. Han, Z. Chen, Y. Tang, *J. Chem. Soc. Chem. Commun.* **1987**, 1076–1077; b) E. Block, M. Gernon, H. Kang, G. Ofori-Okai, J. Zubieta, *Inorg. Chem.* **1989**, *28*, 1263–1271; c) D. M. Knotter, G. van Koten, H. L. van Maanen, D. M. Grove, A. L. Spek, *Angew. Chem.* **1989**, *101*, 351–352; *Angew. Chem. Int. Ed. Engl.* **1989**, *28*, 341–342; d) B. Becker, W. Wojnowski, K. Peters, E.-M. Peters, H. G. Von Schnering, *Polyhedron* **1990**, *9*, 1659–1666; e) E. Block, H. Kang, G. Ofori-Okai, J. Zubieta, *Inorg. Chim. Acta* **1990**, *167*, 147–148; f) D. M. Knotter, H. L. van Maanen, D. M. Grove, A. L. Spek, G. van Koten, *Inorg. Chem.* **1991**, *30*, 3309–3317; g) M. D. Janssen, J. G. Donkervoort, S. B. van Berlekom, A. L. Spek, D. M. Grove, G. van Koten, *Inorg. Chem.* **1996**, *35*, 4752–4763; h) J. A. García-Vázquez, J. Romero, R. Castro, A. Sousa, D. J. Rose, J. Zubieta, *Inorg. Chim. Acta* **1997**, *260*, 221–223.

[10] a) M. Baumgartner, H. Schmalle, C. Baerlocher, *J. Solid State Chem.* **1993**, *107*, 63–75; b) R. V. Parish, Z. Salehi, R. G. Pritchard, *Angew. Chem.* **1997**, *109*, 276–278; *Angew. Chem. Int. Ed. Engl.* **1997**, *36*, 251–253; c) D. Li, T. Wu, X. P. Zhou, R. Zhou, X. C. Huang, *Angew. Chem.* **2005**, *117*, 4247–4250; *Angew. Chem. Int. Ed.* **2005**, *44*, 4175–4178.

[11] a) G. N. Schrauzer, H. Prakash, *Inorg. Chem.* **1975**, *14*, 1200–1204; b) P. Espinet, M. C. Lequerica, J. M. Martín-Alvarez, *Chem. Eur. J.* **1999**, *5*, 1982–1986; c) N. Sandhyarani, T. Pradeep, *J. Mater. Chem.* **2001**, *11*, 1294–1299.

[12] a) J. M. Zuo, M. Kim, M. O'Keeffe, J. C. H. Spence, *Nature* **1999**, *401*, 49–52; b) C. M. Che, Z. Mao, V. M. Miskowski, M. C. Tse, C. K. Chan, K. K. Cheung, D. L. Philips, K. H. Leung, *Angew. Chem.* **2000**, *112*, 4250–4254; *Angew. Chem. Int. Ed.* **2000**, *39*, 4084–4088; c) H. L. Hermann, G. Boche, P. Schwerdtfeger, *Chem. Eur. J.* **2001**, *7*, 5333–5342; d) L. Magnko, M. Schweizer, G. Rauhut, M. Schütz, H. Stoll, H. J. Werner, *Phys. Chem. Chem. Phys.* **2002**, *4*, 1006–1013; e) Z. Mao, H. Y. Chao, Z. Hui, C. M. Che, W. F. Fu, K. K. Cheung, N. Zhu, *Chem. Eur. J.* **2003**, *9*, 2885–2894; f) W. F. Fu, X. Gan, C. M. Che, Q. Y. Cao, Z. Y. Zhou, N. Zhu, *Chem. Eur. J.* **2004**, *10*, 2228–2236.

[13] a) F. Garnier, A. Yassar, R. Hajlaoui, G. Horowitz, F. Deloffre, *Electrochim. Acta* **1994**, *39*, 1339–1344; b) A. Dodabalapur, L. Torsi, H. E. Katz, *Science* **1995**, *268*, 270–271; c) F. Garnier, R. Hajlaoui, A. El-Kassmi, G. Horowitz, L. Laigre, W. Porzio, M. Armanini, F. Provasoli, *Chem. Mater.* **1998**, *10*, 3334–3339; d) A. R. Murphy, J. M. J. Fréchet, P. Chang, J. Lee, V. Subramanian, *J. Am. Chem. Soc.* **2004**, *126*, 1596–1597; e) H. Tian, J. Wang, J. Shi, D. Yan, L. Wang, Y. Geng, F. Wang, *J. Mater. Chem.* **2005**, *15*, 3026–3033.

[14] a) H. Sirringhaus, R. J. Wilson, R. H. Friend, M. Inbasekaran, W. Wu, E. P. Woo, M. Grell, D. D. C. Bradley, *Appl. Phys. Lett.* **2000**, *77*, 406–408; b) J. F. Chang, B. Sun, D. W. Breiby, M. M. Nielsen, T. I. Sölling, M. Giles, I. McCulloch, H. Sirringhaus, *Chem. Mater.* **2004**, *16*, 4772–4776.

[15] a) R. Adams, W. Reifschneider, A. Ferretti, *Org. Synth.* **1962**, *42*, 22–25; b) G. H. Posner, D. J. Brunelle, L. Sinoway, *Synthesis* **1974**, 662–665; c) I. G. Dance, P. J. Guerney, A. D. Rae, M. L. Scudder, *Inorg. Chem.* **1983**, *22*, 2883–2887; d) T. G. Back, S. Collins, M. V. Krishna, K. W. Law, *J. Org. Chem.* **1987**, *52*, 4258–4264; e) M. D. Janssen, D. M. Grove, G. van Koten, *Progress in Inorganic Chemistry, Vol. 46*, Wiley, New York, **1997**, p. 97.

[16] G. Horowitz, *Adv. Mater.* **1998**, *10*, 365–377.

[17] a) P. E. Werner, L. Eriksson, M. Westdahl, *J. Appl. Crystallogr.* **1985**, *18*, 367–370; b) A. Boultif, D. Löuer, *J. Appl. Crystallogr.* **2004**, *37*, 724–731.

[18] G. S. Pawley, *J. Appl. Crystallogr.* **1981**, *14*, 357–361.

[19] a) W. I. F. David, K. Shankland, *DASH*, *Program for Structure Solution from Powder Diffraction Data*, Cambridge Crystallographic Data Centre, Cambridge, **2001**, (License agreement No. D/1023/2002); b) V. Favre-Nicolin, R. Cerný, *FOX*, "*Free objects for crystallography*": A modular approach to ab initio structure determination from powder diffraction, *J. Appl. Crystallogr.* **2002**, *35*, 734–743.

[20] a) B. H. Toby, *EXPGUI, A Graphical User Interface for GSAS, J. Appl. Crystallogr.* **2001**, *34*, 210–221; b) A. C. Larson, R. B. Von Dreele "*General Structure Analysis System (GSAS)*", *Los Alamos National Laboratory Report LAUR 86–748*, **2004**.

[21] a) J. C. Slater, *J. Chem. Phys.* **1964**, *41*, 3199–3204; b) J. Emsley, *The Elements*, Clarendon, Oxford, UK, **1989**, p. 192.

[22] G. Desiraju, T. Steiner, *The Weak Hydrogen Bond in Structural Chemistry and Biology: IUCr Monograph on Crystallography, No. 9*, Oxford University Press, New York, **1999**, pp. 29–121.

[23] S. E. Creager, C. M. Steiger, *Langmuir* **1995**, *11*, 1852–1854.

[24] D. R. Lide, *CRC Handbook of Chemistry and Physics*, 85th ed., **2004**, Chapter 12, pp. 88–89.

[25] a) J. Tauc, R. Grigorovic, A. Vancu, *Phys. Status Solidi. B* **1966**, *15*, 627–637; b) N. A. Hegab, A. E. Bekheet, M. A. Afifi, A. A. El-Shazly, *Appl. Phys. A* **1998**, *66*, 235–240; c) V. Kumar, S. K. Sharma, T. P. Sharma, V. Singh, *Optical Materials* **1999**, 115–119.

[26] a) M. A. Baldo, D. F. O(Brien, Y. You, A. Shoustikov, S. Sibley, M. E. Thompson, S. R. Forrest, *Nature* **1998**, *395*, 151–154; b) A. Tsuboyama, H. Iwawaki, M. Furugori, T. Mukaide, J. Kamatani, S. Igawa, T. Moriyama, S. Miura, T. Takiguchi, S. Okada, M. Hoshino, K. Ueno, *J. Am. Chem. Soc.* **2003**, *125*, 12971–12979; c) Y. L. Tung, P. C. Wu, C. S. Liu, Y. Chi, J. K. Yu, Y. H. Hu, P. T. Chou, S. M. Peng, G. H. Lee, Y. Tao, A. J. Carty, C. F. Shu, F. I. Wu, *Organometallics* **2004**, *23*, 3745–3748; d) H. C. Li, P. T. Chou, Y. H. Hu, Y. M. Cheng, R. S. Liu, *Organometallics* **2005**, *24*, 1329–1335; e) R. C. Evans, P. Douglas, C. J. Winscom, *Coord. Chem. Rev.* **2006**, *250*, 2093–2126.

[27] a) G. Horowitz, X. Z. Peng, D. Fichou, F. Garnier, *J. Mol. Electron.* **1991**, *7*, 85–89; b) C. D. Dimitrakopoulos, A. R. Brown, A. Pomp, *J. Appl. Phys.* **1996**, *80*, 2501–2508.

[28] Z. Bao, A. J. Lovinger, A. Dodabalapur, *Appl. Phys. Lett.* **1996**, *69*, 3066–3068.

[29] a) H. Sirringhaus, P. J. Brown, R. H. Friend, M. M. Nielsen, K. Bechgaard, B. M. W. Langeveld-Voss, A. J. H. Spiering, R. A. J. Janssen, E. W. Meijer, P. Herwig, D. M. De Leeuw, *Nature* **1999**, *401*, 685–688; b) H. Sirringhaus, P. J. Brown, R. H. Friend, M. M. Nielsen, K. Bechgaard, B. M. W. Langeveld-Voss, A. J. H. Spiering, R. A. J. Janssen, E. W. Meijer, *Synth. Met.* **2000**, *111–112*, 129–132; c) J. L. Brédas, J. P. Calbert, D. A. Da Silva Filho, J. Cornil, *Proc. Natl. Acad. Sci. USA* **2002**, *99*, 5804–5809; d) H. Moon, R. Zeis, E. J. Borkent, C. Besnard, A. J. Lovinger, T. Siegrist, C. Kloc, Z. Bao, *J. Am. Chem. Soc.* **2004**, *126*, 15322–15323.

[30] a) F. Garnier, *Electronic Materials: The Oligomer Approach*, Wiley-VCH Verlag GmbH, Weinheim, Germany, **1998**, pp. 559–583; b) D. Holten, D. F. Bocian, J. S. Lindsey, *Acc. Chem. Res.* **2002**, *35*, 57–69.

[31] a) G. Horowitz, R. Hajlaoui, P. Delannoy, *J. Phys. III* **1995**, *5*, 355–371; b) P. V. Necliudov, M. S. Shur, D. J. Gundlach, T. N. Jackson, *J. Appl. Phys.* **2000**, *88*, 6594–6597.
[32] M. C. J. M. Vissenberg, M. Matters, *Phys. Rev. B* **1998**, *57*, 12964–12967.
[33] H. Bässler, *Phys. Status Solidi B* **1993**, *175*, 14–55.
[34] M. Tadokoro, S. Yasuzuka, M. Nakamura, T. Shinoda, T. Tatenuma, M. Mitsumi, Y. Ozawa, K. Toriumi, H. Yoshino, D. Shiomi, K. Sato, T. Takui, T. Mori, K. Murata, *Angew. Chem.* **2006**, *118*, 5268–5271; *Angew. Chem. Int. Ed.* **2006**, *45*, 5144–5147.
[35] P. Nagels, R. Mertens, H. O. Desseyn, *Synth. Met.* **2002**, *128*, 1–6.
[36] a) H. Meng, M. Bendikov, G. Mitchell, R. Helgeson, F. Wudl, Z. Bao, T. Siegrist, C. Kloc, C. H. Chen, *Adv. Mater.* **2003**, *15*, 1090–1093; b) Y. Sakamoto, T. Suzuki, M. Kobayashi, Y. Gao, Y. Fukai, Y. Inoue, F. Sato, S. Tokito, *J. Am. Chem. Soc.* **2004**, *126*, 8138–8140; c) O. Ostroverkhova, D. G. Cooke, S. Shcherbyna, R. F. Egerton, F. A. Hegmann, R. R. Tykwinski, J. E. Anthony, *Phys. Rev. B* **2005**, *71*, 035204.
[37] G. Horowitz, M. E. Hajlaoui, *Synth. Met.* **2001**, *122*, 185–189.
[38] a) M. Shtein, J. Mapel, J. B. Benziger, S. R. Forrest, *Appl. Phys. Lett.* **2002**, *81*, 268–270; b) D. Knipp, R. A. Street, A. Völkel, J. Ho, *J. Appl. Phys.* **2003**, *93*, 347–355.
[39] Y. Sun, L. Tan, S. Jiang, H. Qian, Z. Wang, D. Yan, C. Di, Y. Wang, W. Wu, G. Yu, S. Yan, C. Wang, W. Hu, Y. Liu, D. Zhu, *J. Am. Chem. Soc.* **2007**, *129*, 1882–1883.
[40] a) I. Sunagawa, *Morphology of Crystals*, Terra Scientific Publishing Company, Tokyo, **1987**, pp. 509–587; b) A. Gavezzotti, *Theoretical Aspects and Computer Modeling of the Molecular Solid State*, Wiley, Chichester, UK, **1997**.

Received: May 11, 2007
Revised: January 17, 2008

